BNL-211223-2019-TECH
NSLSII-ASD-TN-291

Complex Bend II

T. Shaftan

October 2018

Photon Sciences
Brookhaven National Laboratory

U.S. Department of Energy
USDOE Office of Science (SC), Basic Energy Sciences (BES) (SC-22)

Notice: This technical note has been authored by employees of Brookhaven Science Associates, LLC under Contract No.DE-SC0012704 with the U.S. Department of Energy. The publisher by accepting the technical note for publication acknowledges that the United States Government retains a non-exclusive, paid-up, irrevocable, world-wide license to publish or reproduce the published form of this technical note, or allow others to do so, for United States Government purposes.

DISCLAIMER

This report was prepared as an account of work sponsored by an agency of the United States Government. Neither the United States Government nor any agency thereof, nor any of their employees, nor any of their contractors, subcontractors, or their employees, makes any warranty, express or implied, or assumes any legal liability or responsibility for the accuracy, completeness, or any third party's use or the results of such use of any information, apparatus, product, or process disclosed, or represents that its use would not infringe privately owned rights. Reference herein to any specific commercial product, process, or service by trade name, trademark, manufacturer, or otherwise, does not necessarily constitute or imply its endorsement, recommendation, or favoring by the United States Government or any agency thereof or its contractors or subcontractors. The views and opinions of authors expressed herein do not necessarily state or reflect those of the United States Government or any agency thereof.

NSLS II TECHNICAL NOTE BROOKHAVEN NATIONAL LABORATORY	NUMBER **NSLSII-ASD-TN-291**
AUTHORS **T. Shaftan, G. Wang, V. Smaluk, Y. Hidaka, O. Chubar, T. Tanabe, J. Choi**	DATE **10/01/2018**
TITLE **Complex Bend II**	

October 1, 2018

Complex Bend II

T. Shaftan, G. Wang, V. Smaluk, Y. Hidaka, O. Chubar, T. Tanabe, J. Choi

Abstract

We present a new optics solution for the Complex Bend [1, 2], which offers to substantially reduce the device length by removing the dipole poles. The bending is now realized by shifting the quadrupole poles along the horizontal axis. The ring optics can be stable if a specific condition on the relationship between the shifts of focusing and defocusing poles is satisfied. This condition is described in Section 2 of this Tech note. Section 1 describes general analysis of beam transport in a shifted quadrupole. Section 3 presents a set of parameters for such a ring, assuming that a single cell of the Complex Bend consists of 2 Combined Function dipoles. Section 4 describes more realistic model of a single cell constructed with two quadrupoles shifted off their reference trajectory. Section 5 is dedicated to calculations of synchrotron radiation from Complex Bend poles. Throughout this preprint we will call the QF-D-B-D-QD-D-B-D version as Complex Bend I (CBI) [1] and the QF-D-QD-D version as Complex Bend II (CBII).

1. General analysis of beam transport in a shifted quadrupole

In this Section we study a cell of CBII that consists of quadrupoles with the "square wave" field distribution along s-axis. A single cell of the CBII contains a focusing quadrupole QF, a drift, a defocusing quadrupole QD and another drift. Bending angle is realized by shifting both quadrupole off-center relative to beam orbit. In our analysis we will be using the following parameters (Table

1):

N_{dip}	Number of dipoles in the ring	60
N_{pdip}	Number of cells per CBII dipole	6
$N_p = N_{pdip} \cdot N_{dip}$	Number of cells in the ring	360
$N_d = 2 \cdot N_p$	Number of poles in the ring	720
$\alpha_d = 2\pi / N_p$	Angle per cell, mrad	17.5
$\alpha_{pdip} = \alpha_d \cdot N_{pdip}$	Angle per CBII element, mrad	105
L_Q	Quadrupole pole length, m	0.187
D_d	Drift length, m	0.03
$L_{cell} = 2 \cdot D_d + 2 \cdot L_Q$	Cell length, m	0.434
$L_{dip} = L_{cell} \cdot N_p$	Complex Bend element length, m	2.604
E, γ	Beam energy, GeV, unitless	3, 5871
BR	Magnetic rigidity, T·m	10.0
K_{1F} / K_{1D}	Scaled gradient in CBII quadrupoles, m^{-2}	50 / -37
$K_{1F,D} \cdot BR$	Corresponding field gradient, T/m	500, -370
AngRatio	Ratio of QF and QD angles over one cell	0.287

Table 1: Parameters used in the analysis of Complex Bend II in this note. Values in the right column are used in the calculations to follow.

The total angle per single cell is distributed between the two quadrupoles according to the parameter 0<*AngRatio* <1. We define the entrance angles as:

$$\Delta xp_F = \frac{\alpha_d}{2} AngRatio, \quad \Delta xp_D = \frac{\alpha_d}{2}(1 - AngRatio),$$

yielding the constraint $2 \cdot (\Delta xp_F + \Delta xp_D) = \alpha_d$. In Figure 1 we illustrate the principle of 1.5 cells of CBII.

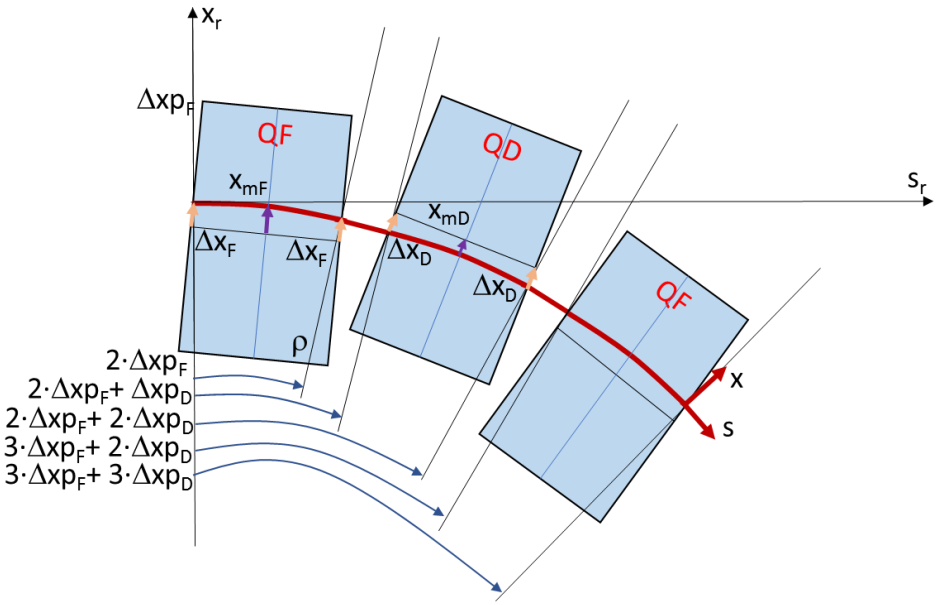

Fig. 1: Sketch of CBII geometry

In the following we include expressions for principle coordinates, trajectories, curvatures and fields along the trajectories. We are separately considering QF and QD quadrupole poles. We use

the following definitions for shortening the expressions:

$$\mu_{0.5QF,D} = 0.5 \cdot \sqrt{K_{1F,D}} \cdot L_Q, \qquad \mu_{QF,D} = \sqrt{K_{1F,D}} \cdot L_Q, \quad \mu_{F,D} = \sqrt{K_{1F,D}} \cdot s,$$
$$C_{0.5Q} = \cos(\mu_{0.5QF}),\ S_{0.5Q} = \sin(\mu_{0.5QF}),\ C_Q = \cos(\mu_{QF}),\ S_Q = \sin(\mu_{QF}),\ C = \cos(\mu_F),\ S = \sin(\mu_F),$$
$$Ch_{0.5Q} = \cosh(\mu_{0.5QD}),\ Sh_{0.5Q} = \sinh(\mu_{0.5QD}),\ Ch_Q = \cosh(\mu_{QD}),\ Sh_Q = \sinh(\mu_{QD}),\ Ch = \cosh(\mu_D),\ Sh = \sinh(\mu_D)$$

Using this notation, we write for the principle coordinates:

$$\Delta x_F = \Delta xp_F \frac{S_Q}{\sqrt{K_{1F}}(1 - C_Q)}, \Delta x_D = \Delta xp_D \frac{Sh_Q}{\sqrt{K_{1D}}(1 - Ch_Q)},$$
$$\Delta x_{mF} = \frac{\Delta x_F}{C_{0.5Q}}, \Delta x_{mD} = \frac{\Delta x_D}{Ch_{0.5Q}}$$

We assume that the trajectory comes in with an angle of $\Delta xp_{F,D}$ with respect to the pole face and leaves the pole with the same angle, so that the trajectory is symmetric relative to the midplane of the pole (Fig. 1). Then we get for the coordinates of the beam trajectory:

$$x_F(s) = \Delta x_F C + \frac{\Delta xp_F}{\sqrt{K_{1F}}} S, \quad x_D(s) = \Delta x_D Ch + \frac{\Delta xp_D}{\sqrt{K_{1D}}} Sh \tag{1}$$

We get the following expressions for the curvatures of trajectories:

$$\rho_{F,D}(s) = \pm \frac{1}{x_{F,D}(s) \cdot K_{1F,D}}, \qquad \rho_{Fav,Dav} = \frac{1}{L_Q} \int_0^{L_Q} \rho_{F,D}(s)\, ds,$$

where ρ_{Fav} and ρ_{Dav} are average radii of trajectory.

The following expressions hold for the fields along these trajectories:

$$B_{F,D}(s) = \frac{BR}{\rho_{F,D}(s)}, \qquad B_{Fav,Dav} = \frac{1}{L_Q} \int_0^{L_Q} B_{F,D}(s)\, ds,$$

where B_{Fav} and B_{Dav} are average fields along the trajectory. We plot the trajectories, curvatures and fields in the next figure.

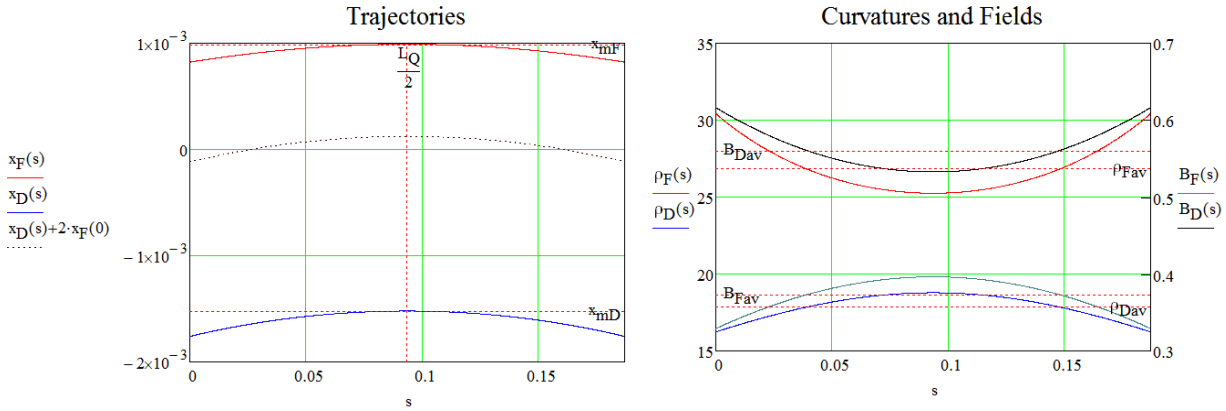

Fig. 2: Trajectories, curvatures and fields along a single pole with the length L_Q.

For finding the length of trajectory through the pole we write:

$$L_{F,D} = 2 \int_0^{0.5L_Q} \sqrt{1 + \Delta x_{mF,D}{}^2 \cdot K_{1F,D} \cdot S^2}\, ds \approx L_Q + \frac{K_{1F,D}{}^2 \cdot L_Q{}^3 \cdot \Delta x_{mF,D}{}^2}{24},$$

where the last expression is obtained by expressing the square root in Taylor series and retaining only the linear term.
Next, we estimate the linear part of the edge focusing. We write for the angle gained by the particle while passing the fringe field of the CBII pole:
For the overall change in focusing due to linear part of the edge fields we get (refer to the sketch of QD pole face on the right):

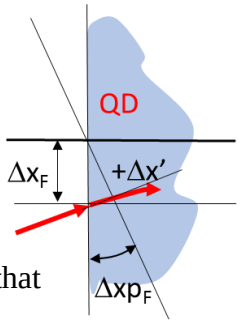

$$\Delta x' \approx \frac{1}{BR}\int_0^{\Delta x_F \Delta xp_F} B(s)ds \approx K_{1F}\,\Delta {x_F}^2 \Delta xp_F,$$

where we assumed that the field along the wedge covered by Δxp_F is constant.
In the "square wave" field model the angle $\Delta x'$ is much smaller (~Δx^3) than that produced by the focusing from the field in the pole's body (~Δx).
Next, we work out the matrices of the quadrupole poles shifted by Δx_F and tilted by Δxp_F, assuming that the trajectory follows equations (1). In this case all terms but the dispersive ones will be the same as for the normal quadrupole.

First, we derive it by referencing trajectory with respect to (1) substituting $K_1 = \sqrt{\frac{K_1}{1+\delta}}$, expanding resulted expression in δ and keeping only terms linear in δ.

$$x(s) = x_o \cos\sqrt{\frac{K_{1F}}{1+\delta}}\,s + x'_o \frac{\sin\sqrt{\frac{K_{1F}}{1+\delta}}}{\sqrt{\frac{K_{1F}}{1+\delta}}}$$

$$\approx x_o C + \frac{x'_o S}{\sqrt{K_{1F}}} + \frac{\delta}{2}\left(-\Delta xp_F\left(L_Q C - \frac{S}{\sqrt{K_{1F}}}\right) + \Delta x_F \sqrt{K_{1F}} L_Q S\right), \qquad (2)$$

where x_o, x'_o are deviations from the reference (1).
We cross-check this expression by directly solving the equation of motion through, for example, a Q_F pole:

$$x'' + K_{1F}x = \frac{\delta}{\rho(s)},$$

where

$$\frac{1}{\rho(s)} = \frac{B(s)}{BR} = K_{1F}\left[\Delta x_F\, C + \frac{\Delta xp_F}{\sqrt{K_{1F}}}S\right].$$

We write the solution in the usual way as

$$x(s) = x_0 y_1 + x'_o y_2 + \delta u(s),$$

and for the inhomogeneous part as:

$$u(s) = y_1 \int \frac{y_2}{\rho(s) W(y_1, y_2)} ds + y_2 \int \frac{y_1}{\rho(s) W(y_1, y_2)} ds,$$

where *W=1* is Wronskian. Integrating, we get the same expression for the dispersive term as in (2).

$$u(s) = -\frac{\Delta x p_F}{2}\left(L_Q C - \frac{S}{\sqrt{K_{1F}}}\right) + \frac{\Delta x_F}{2}\sqrt{K_{1F}} L_Q S$$

As a result of similar analysis, we get the following matrices for the CBII poles in variables (x, x', δ)^T:

$$MF = \begin{vmatrix} C_Q & S_Q/\sqrt{K_{1F}} & -\frac{\Delta x p_F}{2}\left(L_Q C_Q - \frac{S_Q}{\sqrt{K_{1F}}}\right) + \frac{\Delta x_F}{2}\sqrt{K_{1F}} L_Q S_Q \\ -S_Q\sqrt{K_{1F}} & C_Q & \frac{\Delta x_F}{2}\left(\sqrt{K_{1F}} S_Q + K_{1F} L_Q C_Q\right) + \frac{\Delta x p_F}{2}\sqrt{K_{1F}} L_Q S_Q \\ 0 & 0 & 1 \end{vmatrix}$$

$$MD = \begin{vmatrix} Ch_Q & Sh_Q/\sqrt{K_{1D}} & \frac{\Delta x p_D}{2}\left(-L_Q Ch_Q + \frac{Sh_Q}{\sqrt{K_{1D}}}\right) - \frac{\Delta x_D}{2}\sqrt{K_{1D}} L_Q Sh_Q \\ Sh_Q\sqrt{K_{1D}} & Ch_Q & -\frac{\Delta x_D}{2}\left(\sqrt{K_{1D}} Sh_Q + K_{1D} L_Q Ch_Q\right) - \frac{\Delta x p_D}{2}\sqrt{K_{1D}} L_Q S_{hQ} \\ 0 & 0 & 1 \end{vmatrix} \quad (3)$$

where M_{13} and M_{23} are different from these in the transport matrix for the Combined Function magnet with the equivalent $\rho=\rho_{Fav,Dav}$ and $K_{1F,D}$ strengths. A linear transfer matrix for the shifted focusing quadrupole, which is very similar to MF in (3), was also derived earlier with slightly less approximation [3].

For such a magnet we get: M_{13} and M_{23} as:

$$MF_{13} = \frac{1}{\rho_{Fav} K_{1F}}(1 - C), \qquad MF_{23} = \frac{1}{\rho_{Fav} K_{1F}} S$$

for the focusing CFD and the similar expressions for the defocusing CFM:

$$MD_{13} = \frac{-1}{\rho_{Dav} K_{1D}}(1 - Ch), \qquad MD_{23} = \frac{1}{\rho_{Dav} K_{1D}} Sh$$

Substituting values from Table 1 we observe the following difference between CBII and CFM models of a single pole:

	CBII	CFM	(CBII-CFM)/CFM
MF_{13}	5.818136E-4 m	5.783793E-4 m	0.59%
MF_{23}	5.479785E-3	5.447465E-3	0.59%
MD_{13}	1.085286E-3 m	1.081078E-3 m	0.39%
MD_{23}	0.012385	0.012718	-2.62%

Table 2: Comparison between matrix coefficients for CBII and CFM

We conclude that the transport matrices for these two models of the CBII pole are not the same in our case of interest.
Next we describe a single cell of CBII in two ways: $T_F = M_{0.5QF}M_DM_{QD}M_DM_{0.5QF}$ and $T_F = M_{0.5QD}M_DM_{QF}M_DM_{0.5QD}$, where the resulted matrices correspond to maxima and minima of beam envelopes through the element. Using these matrices, we find matched solutions in terms of $\mu, \bar{\beta}_x, \bar{\eta}$ and $\Delta\beta_x, \Delta\eta$.

Then we approximate the beta-function and dispersion trough the cell using expressions like:

$$\begin{bmatrix}\beta_x(s)\\ \eta(s)\end{bmatrix} \approx \begin{bmatrix}\bar{\beta}_x\\ \bar{\eta}\end{bmatrix} + \begin{bmatrix}\Delta\beta_x\\ \Delta\eta\end{bmatrix} \cdot \cos(k_{CB}\mathrm{s}),$$

with $k_{CB} = \frac{2\pi}{L_{cell}}$ These solutions are plotted in Fig. 3.

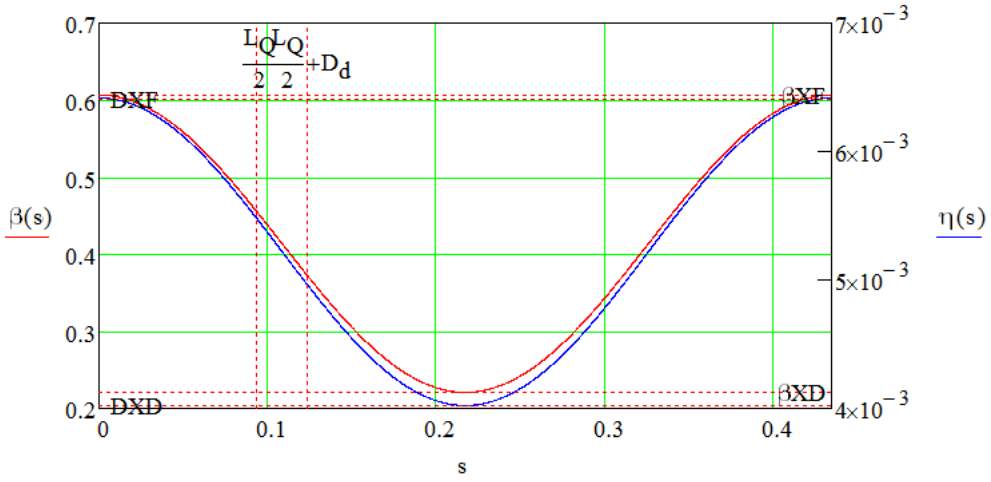

Fig. 3: Approximate solutions for horizontal beta-function and dispersion within a single CBII cell.

With these approximate solutions we find approximate expressions for the storage ring emittance and energy spread.

The average dispersion and beta function in each quad are:

$$\eta_{Fav} = \frac{2}{L_Q}\int_0^{\frac{L_Q}{2}} \eta(s)ds, \qquad \eta_{Dav} = \frac{2}{L_Q}\int_{\frac{L_Q}{2}+D_d}^{L_Q+D_d} \eta(s)ds,$$

$$\beta_{Fav} = \frac{2}{L_Q}\int_0^{\frac{L_Q}{2}} \beta(s)ds, \qquad \beta_{Dav} = \frac{2}{L_Q}\int_{\frac{L_Q}{2}+D_d}^{L_Q+D_d} \beta(s)ds$$

Contribution from the CBII elements to the tune and chromaticity of the whole ring:

$$\nu_x = N_{pdip}\cdot\mu,$$
$$\xi_{x,y} \approx -\frac{N_p}{4\pi}\left(2(K_{1F}-K_{1D})\frac{\Delta\beta_{x,y}}{k_{CB}}\sin\left(\frac{k_{CB}L_Q}{2}\right) \pm (K_{1F}+K_{1D})L_Q\bar{\beta}_{x,y}\right).$$

I_2, I_4 and I_5 are the radiation integral around the ring. Recall that the partition numbers and synchrotron integrals are written as:

$$J_x = 1 - \frac{I_4}{I_2},\ J_z = 2 + \frac{I_4}{I_2},\ I_2 = \oint \frac{ds}{\rho^2}, I_4 = \oint \frac{\eta}{\rho}\left(\frac{1}{\rho^2} + 2K_1\right)ds, I_5 = \oint \frac{H_x}{|\rho|^3} ds$$

The radiation integrals for CBII can be expressed as:

$$\begin{aligned} I_2 &= 2\pi\left(\frac{AngRatio}{\rho_{Fav}} + \frac{(1-AngRatio)}{\rho_{Dav}}\right) \\ I_3 &= 2\pi\left(\frac{AngRatio}{\rho_{Fav}^2} + \frac{(1-AngRatio)}{\rho_{Dav}^2}\right) \\ I_4 &\approx \frac{N_p \cdot \eta_{Fav} \cdot L_Q}{\rho_{Fav}^3} + \frac{N_p \cdot \eta_{Dav} \cdot L_Q}{\rho_{Dav}^3} + \frac{N_p \cdot 2\eta_{Fav} \cdot K_{1F} \cdot L_Q}{\rho_{Fav}} - \frac{N_p \cdot 2\eta_{Dav} \cdot K_{1D} \cdot L_Q}{\rho_{Dav}} \\ I_5 &\approx 2\pi\left(\frac{AngRatio}{\rho_{Fav}^2}\frac{{\eta_{Fav}}^2}{\beta_{Fav}} + \frac{(1-AngRatio)}{\rho_{Dav}^2}\frac{{\eta_{Dav}}^2}{\beta_{Dav}}\right) \end{aligned} \quad (4)$$

The damping partition numbers J are:

$$J_x = 1 - \frac{I_4}{I_2},\ J_z = 2 + \frac{I_4}{I_2}$$

Storage ring emittance and energy spread are [4]:

$$\varepsilon_x = C_q \gamma^2 \frac{I_5}{I_2 - I_4} = C_q \cdot \gamma^2 \cdot \frac{I_5}{J_x \cdot I_2}$$

$$\frac{dE}{E} = \gamma \sqrt{C_q \cdot \frac{I_3}{2I_2 + I_4}}$$

where $C_q \approx 3.84 \cdot 10^{-13}\ m$.

For the momentum compaction we write (approximation valid for $L_Q \gg D_d$):

$$\alpha = \frac{1}{C}\oint \frac{\eta}{\rho} ds \approx \frac{1}{2L_Q}\left(2\int_0^{\frac{L_Q}{2}} K_{1F} \cdot x_F \cdot \eta \cdot ds - \int_{\frac{L_Q}{2}+D_d}^{\frac{3L_Q}{2}+D_d} K_{1D} \cdot x_D \cdot \eta \cdot ds\right)$$

where *C* is the circumference, $K_{1F,D} \cdot \left(\pm x_{F,D}\right) = \frac{1}{\rho_{F,D}}$, and $\eta(s) = \bar{\eta} + \Delta\eta \cdot \cos(k_{CB}\mathrm{s})$, as we have shown in this Section and we considered the cell QF-D-QD-D cell for this expression.

With these expressions in mind we are in position to describe the storage ring lattice along the arcs. All the ring arcs consists of CBII elements, which define the ring optics in terms of emittance, energy spread and momentum compaction and largely affect tunes, chromaticity, driving terms, Dynamic and Momentum apertures.

Before computing these ring parameters, we need to derive an important dependence for the relationship of focusing and defocusing poles in a CBII element. This dependence defines stability of the ring built with CBII elements.

2. Stability constraint for the ring optics based on Complex Bend II

As per expressions from Section 1, J_x is determined by I_2 and I_4, and, in turn, I_2 depends only on the bending radius in dipoles. To maintain the longitudinal or horizontal stability of the beam dynamics in the ring we need to keep J elements of damping distribution always positive. The Complex Bend optics allow us to simplify synchrotron integrals presented above [1]. Following (4), for a sequence of focusing $N_F$and defocusing shifted quadrupole magnets N_D, the 4th synchrotron integral I_4 can be approximated as:

$$I_4 = \int \frac{\eta_F}{\rho_F^3} ds + \int \frac{\eta_D}{\rho_D^3} ds + \int \frac{2\eta_F K_{1F}}{\rho_F} ds + \int \frac{2\eta_D K_{1D}}{\rho_D} ds \approx$$
$$\approx N_F L_F \eta_{Fav} K_{1F}^2 \, \Delta x_F (K_{1F} \Delta x_F^2 + 2) + N_D L_D \eta_{Dav} K_{1D}^2 \, \Delta x_D (K_{1D} \Delta x_D^2 + 2)$$

For the CBII geometry in a GeV range, we expect K_{1F} and K_{1D} to be on the order of 100 $\frac{1}{m^2}$, Δx_F and Δx_D are about 1 mm, so $K_{1F}\Delta x_F^2$ and $K_{1D}\Delta x_D^2$ are ~1e-3 <<2. Change in I_4 due to CBII poles or CFMs can be estimated as:

$$I_4 \approx 2N_F L_F \eta_{Fav} K_{1F}^2 \, \Delta x_F + 2N_D L_D \eta_{Dav} K_{1D}^2 \, \Delta x_D$$

For a periodic structure, $N_F = N_D = N_Q$, $L_F = L_D = L_Q$ he particular case of the no net change in I_4 due to CBII poles or CFMs, we arrive to the relationship between the translations and gradients of the focusing and defocusing poles as:

$$\eta_{Fav} K_{1F}^2 \, \Delta x_F + \eta_{Dav} K_{1D}^2 \, \Delta x_D = 0$$

This constraint maintains ring optics with Complex Bends II stable in all three planes via preserving damping partitions positive. We note that this constraint works for any ring optics that involve combine function magnets or shifted quadrupoles, i.e. CB-II poles.

3. Parameters of Complex Bend II for the case of NSLS-II upgrade

Using the formalism described in Sections 1 and 2 we compared Complex Bend II with the NSLS-II dipole. For the calculations in the Section we adopted a simple model of Complex Bend II, where every pole of the structure is a sector-type Combined Function dipole with the focusing gradient K_1. and the dipole field bending the reference trajectory at the nominal angle per pole (Fig. 4).

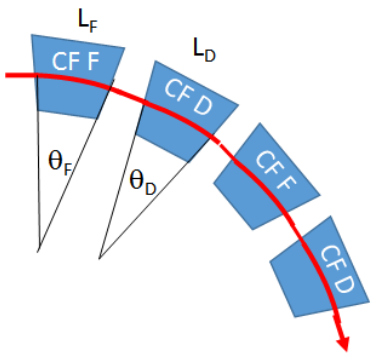

Fig. 4: Optical structure of Complex Bend II approximated by Combined Function dipoles.

Using the Combined Function dipole transport matrix, we calculate matched solutions for Twiss functions and dispersion. Then, with the expressions from the Sections 2 we estimated the ring parameters and optimize it with the technique described in Section 2.

In Table 2 we calculated preliminary parameters of the Complex Bend II as it would be used for the NSLS-II low emittance upgrade.

Number of poles in the ring QF/QD	360/360	Energy, GeV	3.00
Angle per pole in QF/QD, mrad	12.45 / 5	Magnetic field, T, QF/QD	0.267/0.667
Magnetic rigidity, T m	10.00	Bending radius, m, QF/QD	37/15
Number of cells	360	μ_x	0.266
Number of dipoles	60	Shift of ref trajectory per cell, mm	3.79
Number of cells per element	6	$K_{1F,D}$, m^{-2}	50/-37
Angle per dipole, rad	0.105	Magnetic gradient, T/m	500 / -370
Quad Pole length, m	0.187	Bore diameter in quad, cm	1
Drift between poles, m	0.03	Field on bore edge, T	5
Cell length, m	0.434	Shift of quad poles, mm, QF/QD	0.534/1.8

Table 2: Preliminary parameters of a storage ring based on Complex Bend II. Horizontal emittance is 15 pm·rad at 3 GeV.

One of the clear advantages from Complex Bend II, as compared with Complex Bend I, is savings of the overall length of the element structure due to the absence of the dipole poles. Also, now that the structure can be realized with only quadrupole poles, the latter may take longer space. Overall this approach reduces the design complexity of a single cell.

4. Model of the Complex Bend II with shifted quadrupoles

In this Section we analyzed a model of a constant K1 quadrupole with the straight edges. We compared a KQUAD, BMAPXY, BMXYZ in Elegant [5] and the analytical solution (3).

The comparison is presented in Fig. 3 below. We used 3 GeV parameters from the table 2.

	NSLS-II dipole	Complex Bend	70 MeV prototype
Length, m	2.6	2.6	0.58
Bending field, T	0.4	0.267/0.667	0.0187/0.0467
Cell length, cm	-	43.4	14.5
Bending angle per cell, °	6	1	1
$K_{1F,D}$, m^{-2}	0	50/-37	450/-333
Gradient, T/m		500/-370	105/-77.7
β_{max} / β_{min}, m	3.7/0.7	0.56/0.125	0.19/0.042
η_{max} / η_{min}, mm	137/0	4.5/2.6	1.5/0.86

Table 3: Parameters of NSLS-II dipole and Complex Bend used in the calculation.

The trajectories calculated with Elegant (Fig. 5) agrees with the theoretical estimates to about 10^{-9}…10^{-7} meters.

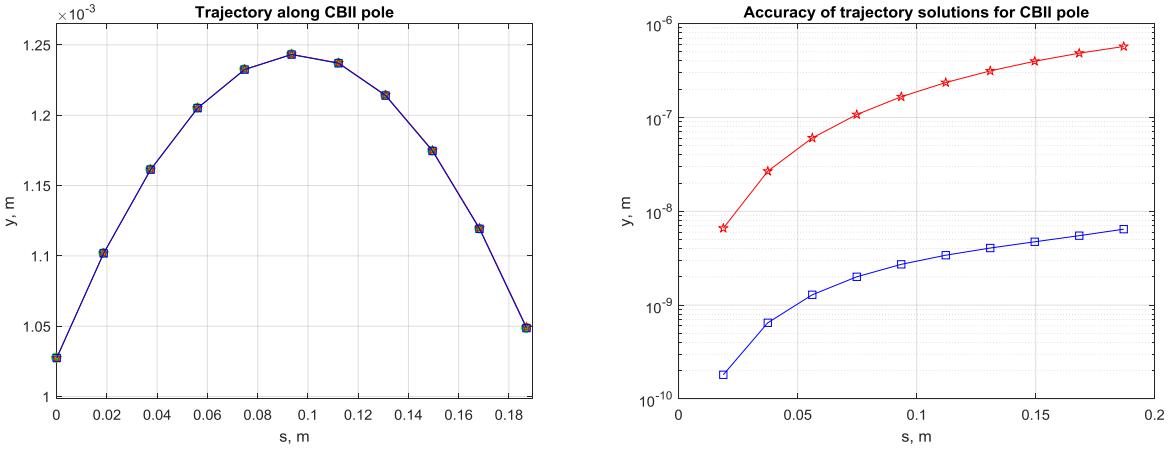

Fig. 5: Left figure: comparison of analytic calculation (blue) with BMXYZ and (2) for δ=3%. Right figure shows the difference between results obtained with BMXYZ in the Elegant model and theoretical calculation (blue squares), together with results from BMXYZ and linearized theoretical calculation (red stars, (2)).

As follows from the study above, the first order estimate (3) describes the particle motion through the shifted quadrupole with the accuracy adequate for the calculations of horizontal beta-function and linear dispersion that we need for the emittance calculation.

In Table 3 we also calculated parameters of the Complex Bend prototype for future ATF experiments at the beam energy of 70 MeV. The CBII prototype will be 62 mm long and consist of 4 cells with the field gradient at 100 T/m. We scaled complex bend parameters from the energy of 3 GeV to that of 70 MeV, which corresponds to reduction in magnetic rigidity (*BR*) by a factor of C_E=0.023. In this scaling we reduced the element length by a factor of C_L=3, including quadrupole length and drift in between the poles, while keeping the values of bend angle and tune the same as for the 3-GeV CBII cell. Thus, overall, the cell length scales down by a factor of C_L and becomes 14.5 cm. The bending field scales down according to *BL/BR*, so the dipole field from both quadrupoles reduce by a factor of C_E/C_L~14.3 versus the 3-GeV CBII cell. The quadrupole K_1 changes according to $\sqrt{K_1}L_Q$ to maintain the same tune per cell, increasing by a factor of C_L^2=9

and the quadrupole gradient changes according to K_1/BR (reduction by a factor of C_E/C_L^2=4.76). Consequently, beta-function and dispersion scale down by a factor of 3.

In reality we have much more complex fields that deviate from the "square-wave model" above. Fig. 6 presents the 3D field map of a single focusing pole calculated with the program RADIA [6].

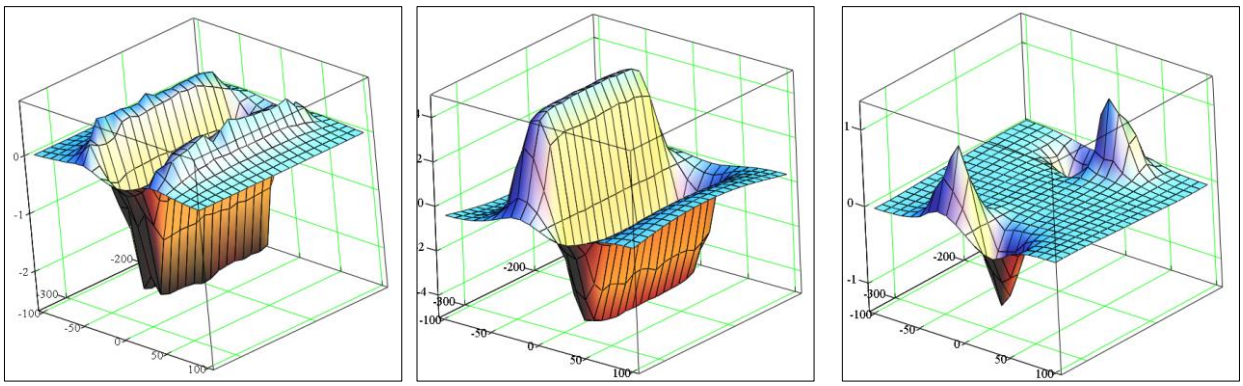

Fig. 6: Realistic field (T) distributions of a Complex Bend pole in coordinates x and z at y=5mm.

A comparison CBI with CBII brings an interesting thought of the advantage in having quadrupole fringe fields of poles of alternative polarity in close proximity to each other. This is true only for CBII and may help in cancelling the nonlinear kicks from the neighboring poles.
As a part of future work, we will be loading this map to ELEGANT to compute particle dynamics by tracking and evaluate nonlinear effects coming from 3D field distribution.

5. Calculations of synchrotron radiation from a Complex Bend

Here we estimate general radiation properties from the CBII element as it has been installed in a 3 GeV ring (Table 4).

Critical wavelength, λ_c	5.56 A
Critical photon energy, ε_c	2.23 keV
SR opening half angle at critical wavelength λ_c	0.17 mrad
SR half spot size at critical wavelength at CBII exit	0.44 mm
Energy loss per revolution	335.3 keV
Radiated power in the ring (0.5A)	167.6 kW
Radiated power per dipole	2.6 kW

Table 4: Synchrotron Radiation properties of CBII and the ring based on CBII lattice.

We introduced the sequence of Complex Bend poles into Synchrotron Radiation Workshop [7]. The next figure 7 presents with a calculation of the synchrotron radiation emitted in the Complex Bend element that consists of 5 poles.

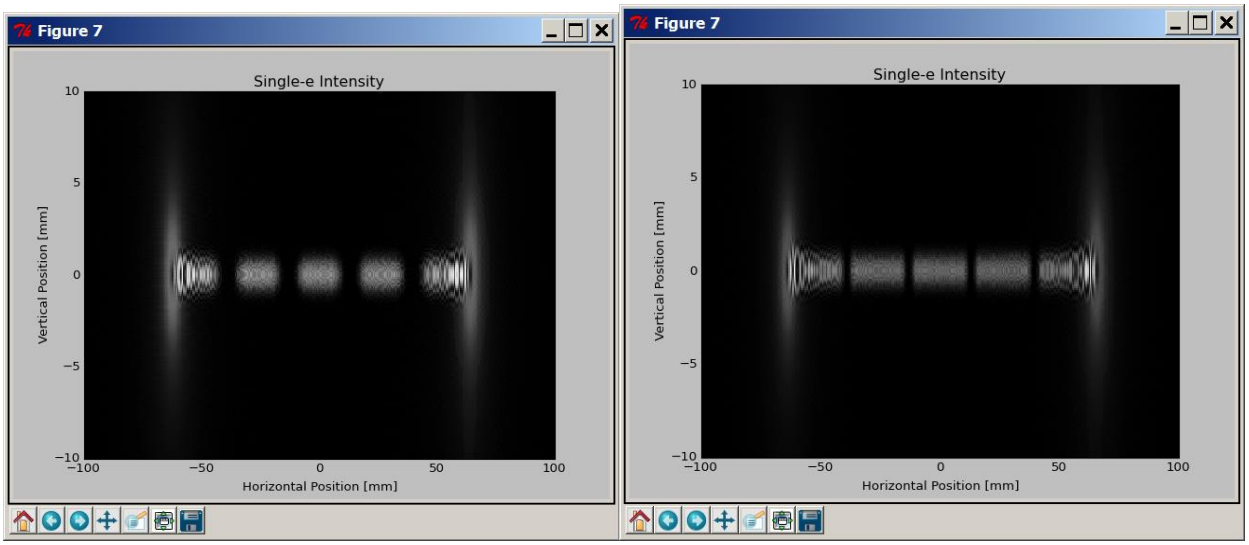

Fig. 7: Calculation of synchrotron radiation power from the Complex Bend at 10 keV. The radiation is sampled 10 meter away. Left figure corresponds to the case of 1 cm field roll-off in the poles, while the right figure plots the intensity distribution with that of 2.5 cm.

The radiation pattern consists of lobes corresponding to intensity peaks from separate poles in the Complex Bend structure. The fuzzy spots on the edges of the distribution are artifacts of the calculation.

In the next example we show how to integrate a superbend into the Complex Bend element. In the calculation below the field of the center pole is increased to 4.3T, comparable with the peak field of NSLS-II HEX wiggler (Fig. 8).

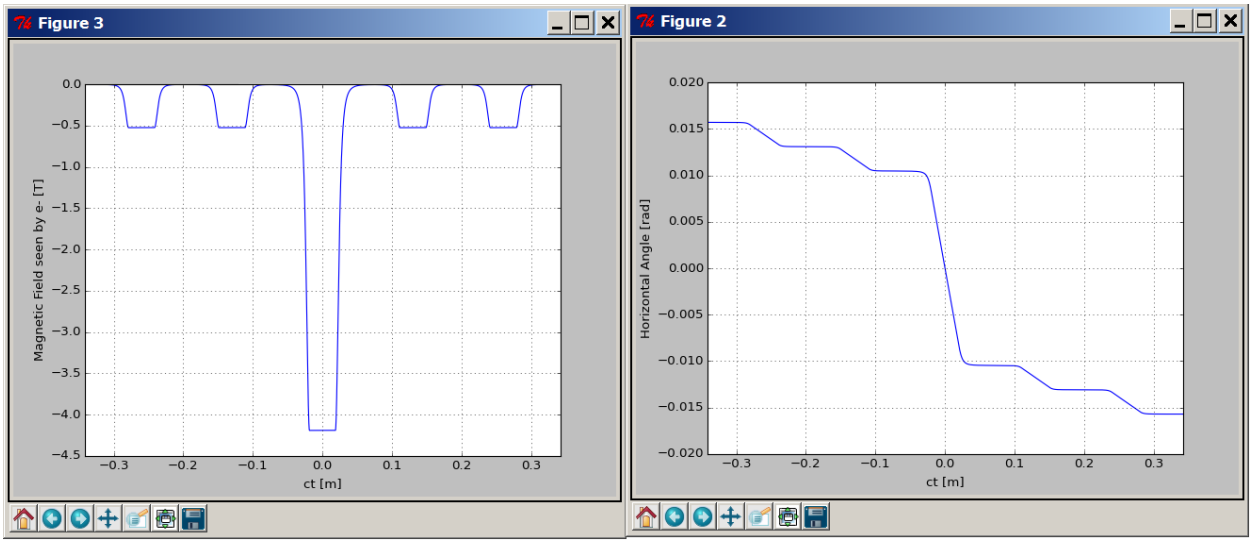

Fig. 8 : Magnetic field distribution (left plot) and angle of beam trajectory through the CBI element (right plot).

Power distribution in the far zone is much wider and overlaps with that from neighboring poles. (Fig. 9).

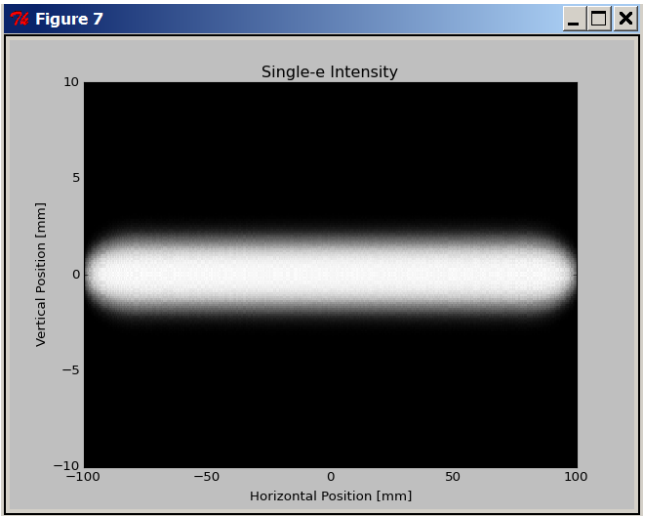

Fig. 9: Intensity distribution from CBI with the superbend as a single high-field pole in the middle of the element.

6. Conclusion

In this note we presented analysis of the Complex Bend II geometry wherein the magnetic structure of the bend consists of only quadrupole poles alternating polarity with shifts of poles in the horizontal direction to acquire the required bending. We first derived a condition for these shifts in focusing and defocusing poles, then worked out an example of replacing the NSLS-II bends with the elements of the Complex Bend II type. Our constraint works for any ring optics that involve combine function magnets or shifted quadrupoles, i.e. CB-II poles.

Next, we studied several models of a single pole of Complex Bend II using analytic estimates and tracking codes and estimated Twiss parameters and dispersion in the cell. We calculated all basic parameters of the ring, based on the CBII concept and confirmed them with ELEGANT/MAD calculations. We concluded this note with simulations of synchrotron radiation from the Complex Bend structure.

The Complex Bend project is now funded by NSLS-II Improvement program for implementation in FY19 and FY20. A prototype will be developed for magnetic measurements and testing with beam at BNL's ATF at 70 MeV. We developed and presented in this note the scaling laws for the prototype.

7. Acknowledgements

Timur Shaftan thanks Barbara Moebes for typing many formulas in this manuscript.

8. References

[1] T. Shaftan, V. Smaluk and G. Wang, The Concept of Complex Bend, NSLS-II Tech note 276, Jan 2018
[2] G. Wang *et al.*, Complex bend: Strong-focusing magnet for low-emittance synchrotrons, accepted in PR AB, Sept 2018
[3] Private communication with Y. Hidaka

[4] S.Y. Lee, Accelerator Physics (Third Edition)
[5] M. Borland, "elegant: A Flexible SDDS-Compliant Code for Accelerator Simulation," Advanced Photon Source LS-287, September 2000
[6] RADIA, O. Chubar, http://www.esrf.eu/Accelerators/Groups/InsertionDevices/Software/Radia
[7] SRW, O. Chubar and P. Elleaume, http://www.esrf.eu/Accelerators/Groups/InsertionDevices/Software/SRW